



Full length article

Near 5% DMSO is the best: A structural investigation of PEDOT: PSS thin films with strong emphasis on surface and interface for hybrid solar cell

Somnath Mahato^{a,b,*}, Joaquim Puigdollers^b, Cristobal Voz^b, Mala Mukhopadhyay^a, Manabendra Mukherjee^a, Satyajit Hazra^{a,**}^a Saha Institute of Nuclear Physics, 1/AF Bidhannagar, Kolkata 700064, India^b Department of Electronic Engineering, Universitat Politècnica de Catalunya, Barcelona 08034, Spain

ARTICLE INFO

Keywords:

PEDOT:PSS
DMSO doping
Morphology
Conductivity
Hybrid solar cell

ABSTRACT

Effect of dimethyl sulfoxide (DMSO) doping on poly(3,4-ethylenedioxythiophene)-poly(styrenesulfonate) (PEDOT:PSS) thin films have been optimized for obtaining better hole transport layer in hybrid solar cell. The correlation between morphology and conductivity is established through atomic force microscopy and transmission length method measurements. On the other hand, change in the shape of the building blocks (from spheroidal-like to ellipsoidal-like) in the PEDOT:PSS films with DMSO concentration is apparent from their electron density profiles and topographies, suggesting possible conformational change (from coil-like to rod-like) in film by X-ray reflectivity. Such change is further evident from their compositional profiles, work functions and electronic band structures estimated from X-ray and ultraviolet photoelectron spectroscopies. In fact, complementary information suggest that near 5% DMSO doped PEDOT:PSS film is governed through maximum in-plane extended ellipsoidal-like blocks as well as well-organized in out-of-plane ordering which is likely to be the optimum structure for increased the highest electrical conductivity up to 1230 S/cm. Finally, maximum power conversion efficiency of 11% with open-circuit voltages around 600 mV, a short-circuit current density higher than 30 mA/cm² and a fill factor of 59.4% is achieved for the 5% DMSO doped PEDOT:PSS/n-Si hybrid solar cell, which is perfectly correlated with their structure.

1. Introduction

Silicon technology is the most dominant photovoltaic technology due to its excellent performance with high power conversion efficiency (PCE) and long-term stability. However, the fabrication of crystalline silicon (c-Si) solar cell requires many deposition processes with high production cost. Therefore, hybrid photovoltaic devices based on the combination of organic and inorganic semiconductors are currently under research as an approach to next generation photovoltaic application, because of its easy fabrication process and less production cost. [1,2] Thus the use of conductive polymer as an organic material is an attractive approach due to the possibility of using low temperature and cost-effective techniques, such as spin coating [3], spray-pyrolysis [4] and ink-jet printing [5] etc. Such organic/inorganic hybrid solar cell can be fabricated at moderate temperatures (< 150 °C), which indicates reduced production cost and without degradation of the minority carrier lifetime of the crystalline silicon.

Poly(3,4-ethylenedioxythiophene):poly(styrenesulfonate)

(PEDOT:PSS) is one such composite polymers, which is highly conductive, transparent, flexible semiconductor. PEDOT is based on 3,4-ethylenedioxythiophene (EDOT) monomer that carries electrical positive charges, but showing low water solubility, whereas PSS carries negative charges but fully soluble in water. Thus, PEDOT compound is usually mixed with PSS to enhance the whole solubility in water. As a result, it is possible to deposit on the desired surface by different solution-based coating techniques. [6–8] The solution-based PEDOT:PSS thin films have been investigated by many research groups [9–11] as an alternative hole-selective contact in crystalline silicon solar cells due to its high transparency and high electrical conductivity.

The electrical conductivity of the PEDOT:PSS thin film depends on the percentage of PSS content. With the increase of PSS content the conductivity decreases [12] because of its insulating behavior. To increase the conductivity of PEDOT:PSS different high boiling point co-solvents are used. Recently it has been reported that the use of dimethyl sulfoxide (DMSO) [13], ethylene glycol (EG) [14] or methanol (MeOH) [15] can increase the electrical conductivity of the final compound

* Correspondence to: S. Mahato, Saha Institute of Nuclear Physics, 1/AF Bidhannagar, Kolkata 700064, India.

** Corresponding author.

E-mail addresses: som.phy.ism@gmail.com (S. Mahato), satyajit.hazra@saha.ac.in (S. Hazra).

layers up to 2 or 3 orders of magnitude. [16,17] To date, the best results have been obtained by using DMSO co-solvent. The morphological change of the PEDOT:PSS structure before and after the addition of DMSO was investigated by many groups. [18,19] It has been reported (Thomas et al. [20]), before addition of DMSO with PEDOT:PSS solution, the oblate-ellipsoidal shaped PEDOT domains are amalgamated in the PSS matrix. Instantly, the PSS chains are aligned along the surface and the benzoic components are coil-like randomly oriented near the grain boundary regions. After addition of DMSO, the packing density of PEDOT:PSS is enhanced and produces clustering with decreased PSS content at the surface. As a result, randomly oriented PEDOT:PSS domains are distributed directed in a particular direction (perpendicular to the surface) Meanwhile, Lee et al. [21] investigated the addition of DMSO, which show enhancement of cohesion and electrical conductivity due to the inter-PEDOT bridging mechanism. Subsequently, different types of surfactant such as Capstone FS-31 [22], Capstone FS-30, Triton [23], Zonylfluoro [24] etc. have been used to increase the wettability of PEDOT:PSS solution. Also the wettability of PEDOT:PSS with silicon surface was found to play an important role in controlling the quality of the hole-selectivity character of the PEDOT:PSS/*n*-Si hybrid solar cell. Maximum PCE for hybrid PEDOT:PSS/*n*-Si solar cell reported by Nagamatsu et al. [25] is 12% (16 mm² active cell area in textured silicon wafers). Thomas et al. [26] achieved highest PCE of 14.6% (49 mm² active cell area), optimizing the mixture of EG and MeOH co-solvent concentration and in combination with different commercial surfactants. Although, lot of study for the DMSO doped PEDOT:PSS have been found in the literature, but there still lack a clear correlation between their charge transport property and the structures. It is needless to say that understanding such correlation is very important for the performance of PEDOT:PSS thin film as a hole selective contact in organic/inorganic hybrid solar cell.

In this present work, the influence of DMSO concentration (2.5, 5 and 7.5 vol%) on the morphology and electrical conductivity of the PEDOT:PSS films, namely, the open circuit voltage and sheet resistance of hybrid solar cells, were investigated. First, significant changes in the film-thickness and electron density profiles were established from the synchrotron-based X-ray reflectivity (XR) study. Then a possible morphological model of the PEDOT:PSS films after the addition of DMSO was sketched, based on the atomic force microscopy (AFM) and XR studies. The composition changes regarding the PEDOT-to-PSS ratio, which are expected to have a positive influence on electrical conductivity was obtained from the transmission length method (TLM), while the interface property of PEDOT:PSS/*n*-Si was obtained from the X-ray photoelectron spectroscopy (XPS) and ultraviolet photoelectron spectroscopy (UPS). Finally, an organic/inorganic hybrid solar cells have been fabricated using crystalline silicon as light absorber, optimized PEDOT:PSS as a hole transport layer (HTL) and *n*-doped hydrogenated amorphous silicon as electron transport layer (ETL).

2. Results and discussion

2.1. X-ray reflectivity and electron density profile

XR data (R) normalized with Fresnel's reflectivity (R_F) for the spin-coated PEDOT:PSS thin films on *n*-Si substrates for different DMSO concentrations are shown in Fig. 1. The signature of the critical wavevector (q_c) for both the film ($q_{c, \text{film}}$) and the substrate ($q_{c, \text{sub}}$), which are the measure of their respective average electron densities, are clearly observed for all three films. Also, the oscillations or Kiessig fringes, which are the measure of the total film thickness, are very clearly evident in all the XR profiles. The frequency and amplitude of the Kiessig fringes, however, vary with the DMSO concentration. To obtain the quantitative information about the PEDOT:PSS thin films, all XR profiles have been analyzed using Parratt's formalism [27] after incorporating roughness at each interface [28]. An instrumental resolution in the form of a Gaussian function was included at the time of data

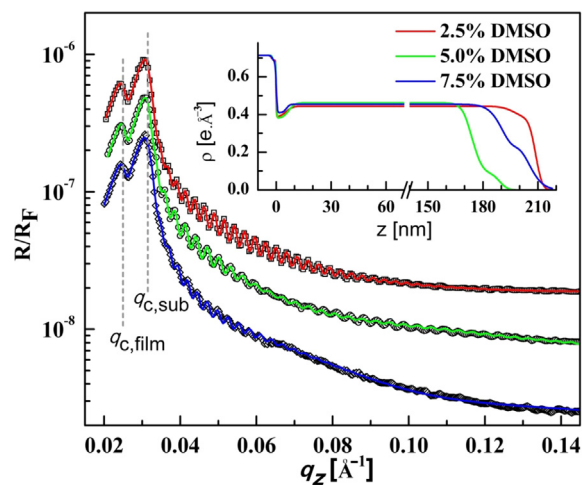


Fig. 1. Normalized XR data (different symbols) and analyzed curves (different color solid lines) of different DMSO doped PEDOT:PSS thin films on Si substrates, spin-coated at fixed speed (1 k rpm). Curves are shifted vertically with respect to each other for clarity. The positions of the q_c for the film and the substrate are indicated. Insets: the corresponding analyzed EDPs.

analysis. For the analysis, each film was divided into 3 layers, as a single layer above the substrate cannot fit the data. Also, the 3-layer model is more realistic as it can incorporate the possible variation at the film-substrate and film-air interfaces with respect to the rest of the film. The best fit XR profiles along with the corresponding EDPs for all the PEDOT:PSS thin films are shown in Fig. 1.

Appreciable change in the film-thickness with DMSO concentration is observed in the EDPs (Fig. 1) of the films. Such change in thickness is partially compensated by the change in the corresponding electron density. The change in these two parameters indicates some change in the internal structure of the films. Minimum thickness ($\sim 180 \pm 10$ nm) is found for the 5% DMSO doped PEDOT:PSS film, while maximum thickness ($\sim 210 \pm 5$ nm) is found for the 2.5% DMSO doped PEDOT:PSS film. The change in thickness can be associated with the change in the shape of the building blocks in the film. The low thickness can arise from ellipsoidal building blocks (with compression along out-of-plane direction and elongation along in-plane direction), while large thickness can arise from spheroidal building blocks. The intermediate thickness ($\sim 195 \pm 12$ nm) for the 7.5% DMSO doped PEDOT:PSS film can be due to the similar ellipsoidal building blocks but with different elongation direction (i.e. with some tilt). Such possible change in the shape and/or tilt of the building blocks with DMSO concentration is quite interesting as the in-plane elongated blocks are expected to enhance the in-plane electrical transport properties of the film. Accordingly, best in-plane transport is expected for the 5% DMSO doped PEDOT:PSS thin film.

No appreciable changes are observed in the film-substrate interfacial region with DMSO concentration but appreciable change in the top surface roughness is observed in the EDPs (Fig. 1 insert) of the films. Such change in the roughness (mainly arising from steps) seems to correlate more with coverage of the building blocks. The top surface coverage for the 2.5% DMSO doped PEDOT:PSS thin film is found maximum, while that for the 5% DMSO doped PEDOT:PSS thin film is found minimum. Although, that coverage for the 7.5% DMSO doped PEDOT:PSS thin film is in between, the tilted ellipsoidal building blocks seem to give rise maximum top surface roughness. The low top surface coverage, which is observed for the 5% DMSO doped PEDOT:PSS thin film prepared at 1 k rpm, is found to increase with the spinning speeds (Fig. S1 in the Supporting Information). This possibly suggests weak long-range interaction along out-of-plane direction as the film thickness drastically decreases (from 180 nm to 75 nm) with the increase in the speed (from 1 k rpm to 3 k and 4 k) rpm. At low speed, the blocks on the

top surface are quite far from the substrate and expected to feel weak interaction, which may lead some of them to slip out. While at high speed, the blocks on the top surface are relatively close to the substrate and thus expected to feel relative strong interaction, which may restrict them from slipping out.

2.2. Atomic force microscopy and topography

The surface morphology predicted by XR data analysis can be verified or complemented by directly looking at the topography of the film through AFM technique. The AFM images (as shown in Fig. S2 (a)-(c) in the Supporting Information) suggest that all films are composed of domains or blocks. The size and shape of such domains are however found different for the different films. The average domain length for the films with 2.5, 5 and 7.5% DMSO are found in the range 75–100, 200–230 and 100–125 nm, respectively. Maximum domain length of ~230 nm is observed for the 5% DMSO doped PEDOT:PSS thin film. Similar phenomenon was previously observed by Mengistie et al. [29] when they added ethylene glycol (EG). In the corresponding phase images (as shown in Fig. S2 (d)-(f) in the Supporting Information) the dark and bright regions indicate the PSS and PEDOT phases [21].

The information about the surface height-fluctuation and surface roughness in the films are better obtained from the bearing plots [31,33] of the AFM images and their derivative plots as shown in Fig. 2. The height-fluctuation is found maximum for the 2.5% DMSO doped PEDOT:PSS thin film, minimum for the 5% DMSO doped PEDOT:PSS thin film and intermediate for the 7.5% DMSO doped PEDOT:PSS thin film. Similar trend is also observed for the surface roughness or standard deviation (σ), obtained from the fitting of the derivative profiles with the Gaussian functions, namely $\sigma \approx 3.8, 2.4$ and 3.1 nm for the 2.5%, 5% and 7.5% DMSO doped PEDOT:PSS thin films, respectively. The low σ -value for the 5% DMSO doped PEDOT:PSS thin film is consistent with the out-of-plane compact and in-plane extended domain morphology of the film. The morphology of the films as predicted from EDPs and topographies are shown schematically in Fig. 3 (a)-(c). It can be noted that similar morphological model was described by Rivnay et al. [30] when EG was used instead of DMSO. The coulombic attraction between PEDOT and PSS chains is expected to reduce with the increase of DMSO concentration, which may lead to the change in the PEDOT conformation from coil-like to extended-coil-like (i.e. from benzoid to quinoid) and change in the shape of the domains (from spheroidal to ellipsoidal). Such asymmetric domains (of PEDOT:PSS) are known to have thinner boundaries (of PSS) and hence less energy barrier and increase hole injection [31]. However, orientation or tilt of the domains is important for achieving better in-plane transport

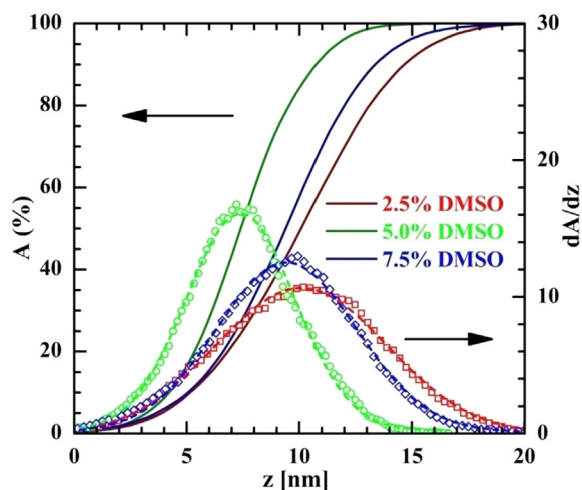


Fig. 2. Bearing area (A) and its derivative (dA/dz) as a function of height (z), as obtained from AFM images, for different DMSO doped PEDOT:PSS thin films.

properties. The extended in-plane domains (least tilt) with reduced energy barrier is proposed for the 5% DMSO doped PEDOT:PSS thin film, which is expected to create easy hole movements from domains to domains along in-plane direction.

2.3. X-ray and ultraviolet photoelectron spectroscopies

XPS measurements have been performed to study the charge transfer properties of the polymer (PEDOT:PSS) thin films prepared at different co-solvent (DMSO) concentration. The survey scan of XPS spectra of PEDOT:PSS with different DMSO concentration films are shown in Fig. 4(a). The peaks corresponding to C1s, O1s and S2p band shows the chemical bonding among carbon-carbon (C–C), carbon-hydrogen (C–H) carbon-sulfur (C–S), oxygen-hydrogen (O–H) and sulfur-oxygen (S=O) atoms [32]. For C 1s spectra, [shown in Fig. 4(b)] the peak at 284.4 eV is assigned to C–C/C–H bonds and the peak at 285.9 eV corresponds to C–S bonds. Besides, the broad peak at 291.9 eV indicated π - π^* shake up transition which is in agreement with previously reported results by H. K. Park et al. [33] and D. J. Yun et al. [34]. The O 1s spectra clearly shows the two peaks correspond to S=O bands (lower energy) and O–H bands (higher energy) respectively shown in Fig. 4(c). Figure, 4(d) shows the deconvolution of S2p spectra corresponding to doublets of S2p_{3/2} and S2p_{1/2} with spin-orbit splitting of 1.1 eV. The higher binding energy peak (167.5–169.3 eV) indicates the sulfur in the sulphonic acid of PSS and lower binding energy peak (163.4–165.3 eV) indicates the sulfur in the thiophene ring of PEDOT. There is an overall peak shift in O1s and S2p spectra [shown in Fig. 5(b) and 5(c)] towards the higher binding energy for 5% and 7.5% DMSO sample with respect to 2.5% DMSO concentration. On the other hand, the shift of C1s spectra is negligible, however there is a small shift towards the lower binding energy (~0.1 eV) in 5% DMSO doped PEDOT:PSS thin film as shown in Fig. 5(a). It appears that with the increase of DMSO concentration (5% and 7.5%), the polymer chains aligns as dipoles on the film surface which induces a positive environment for the S and O atoms and a negative environment for the C atoms of the polymer. The negligible shift for C1s spectra may be explained in the terms of saturated environment of the C atom in the polymer. Due to the presence of these dipoles, the holes generated (in presence of light) in the *n*-Si is transferred more efficiently to the HOMO level of PEDOT:PSS. The F1s spectra comes from the Capstone FS-31 which is considered to be physically mixed with the PEDOT:PSS domains without having any chemical interaction with it. The positive peak shift (~0.8 eV) of F1s spectra [shown in Fig. 5(d)] towards the higher binding energy with the increase of higher DMSO concentration can be explained in the terms of the effect of dipolar interaction with the capstone molecules. In addition, small N 1s peak is found due to imidazolium cation which may interacts with sulfonic acid group of PSS chains and neutralized. The integral area ratio of PSS/PEDOT obtained from S2p peak is found to be minimum (2.43) for 5% DMSO. Whereas the other two ratios are 2.65 and 2.53 for 2.5% and 7.5% DMSO concentration respectively. As the PSS content is less in 5% DMSO, it suggests that the overall PSS thickness is less on PEDOT:PSS domain which justifies our XRR results.

Now we used Ultra-violet Photoelectron Spectroscopy (UPS) to study the correlation between domain structure and the molecular electronic states which play a significant role in the energy band alignment of PEDOT:PSS/*n*-Si heterojunction. We carried out UPS measurements by using a helium lamp emitting at excitation energy of 21.6 eV of PEDOT:PSS/*n*-Si interface and evaluated the work function (Φ) and the highest occupied molecular orbital (HOMO) level. Fig. 6(a) describes the UPS spectra of PEDOT:PSS/*n*-Si heterojunction. The work function was determined from the difference between the excitation energy of 21.6 eV and the binding energy at the position of the secondary electron cut-off (SECO). Fig. [6(a) (insert)] shows the secondary cut-off region of 2.5, 5 and 7.5% DMSO doped PEDOT:PSS polymer films as 15.92, 16.03 and 16.0 eV respectively. Thus, the estimated

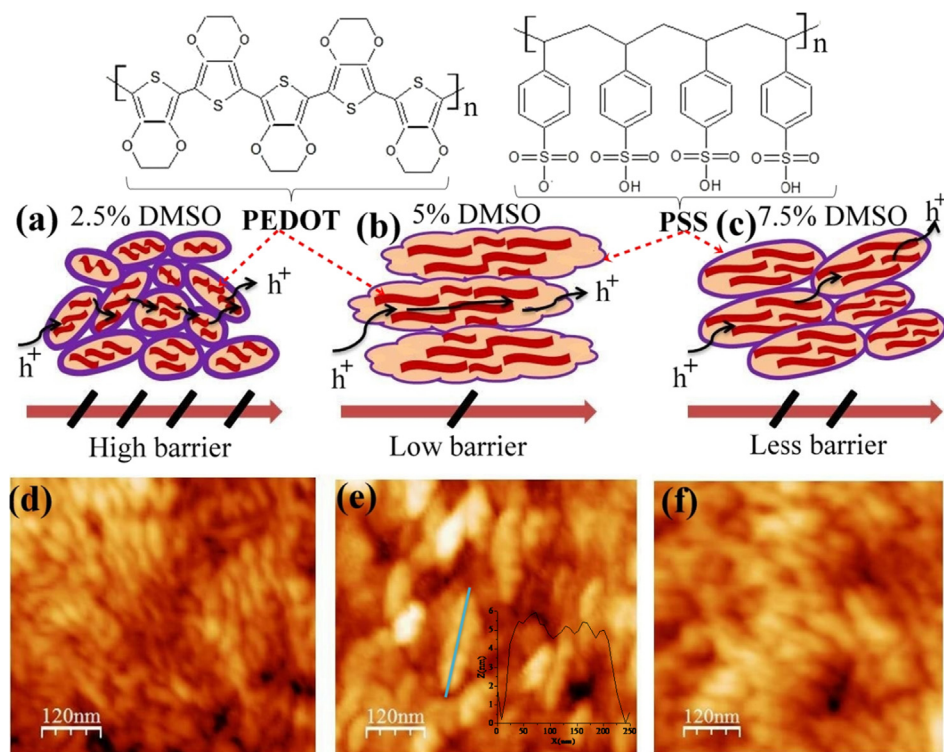


Fig. 3. [(a), (b), (c)]: Schematic morphological models of spin-coated PEDOT:PSS (doped with 2.5, 5 and 7.5% DMSO), [(d), (e), (f)] shows the topological image of PEDOT:PSS domain after the addition of DMSO and insert shows the line profile of PEDOT:PSS domain in 5% DMSO doped PEDOT:PSS thin film optimizing maximum domain length of 230 nm.

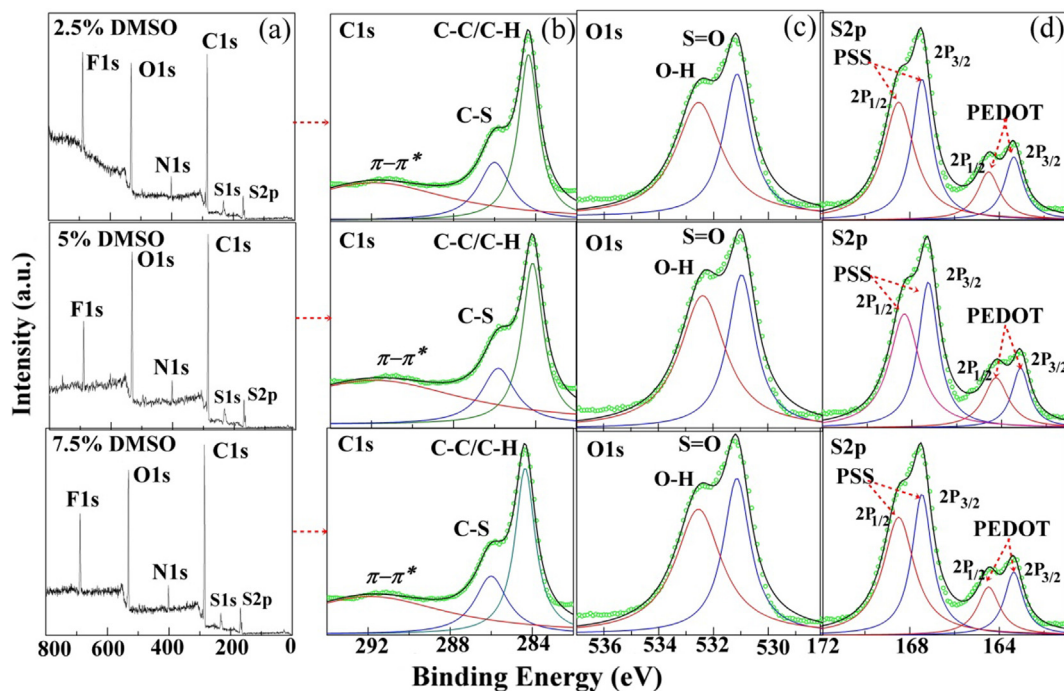


Fig. 4. Chemical composition analysis of the DMSO doped PEDOT:PSS thin film using X-ray photoelectron spectrometry: (a) survey scan of XPS spectra, (b–d) deconvolution of C 1s, O 1s and S 2p core level of PEDOT:PSS with 2.5, 5, and 7.5% DMSO doped thin films.

work function of those films are 5.68, 5.57 and 5.60 eV which is in good agreement with values reported by other research groups [35,36]. Our XPS analysis confirms that the PSS-to-PEDOT ratio at the surface is minimum in 5% DMSO doped PEDOT:PSS film, which may be responsible for decreasing the work function of PEDOT:PSS thin film, similar results have been reported by Kim et al. [37]. On the other hand the HOMO level (for 5% DMSO sample) is shifted maximum by about 0.3 eV towards the higher binding energy compared to 2.5% DMSO doped PEDOT:PSS thin film, which is illustrated in Fig. 6(b) (insert).

The shift of HOMO level is responsible for the formation of interface dipole between PEDOT:PSS and *n*-Si as mentioned above. The strength of the interface dipole has been calculated with the following relation:

$$\psi\Delta = -(eD + V_d) \quad (1)$$

where eD is the interface dipole, V_d is the band bending estimated from the shift of HOMO level and $\psi\Delta$ is the work function shift with respect to 2.5% DMSO sample. Evaluated interface dipole for 5% DMSO doped PEDOT:PSS film is (0.41 eV) larger than that of 7.5% DMSO doped film

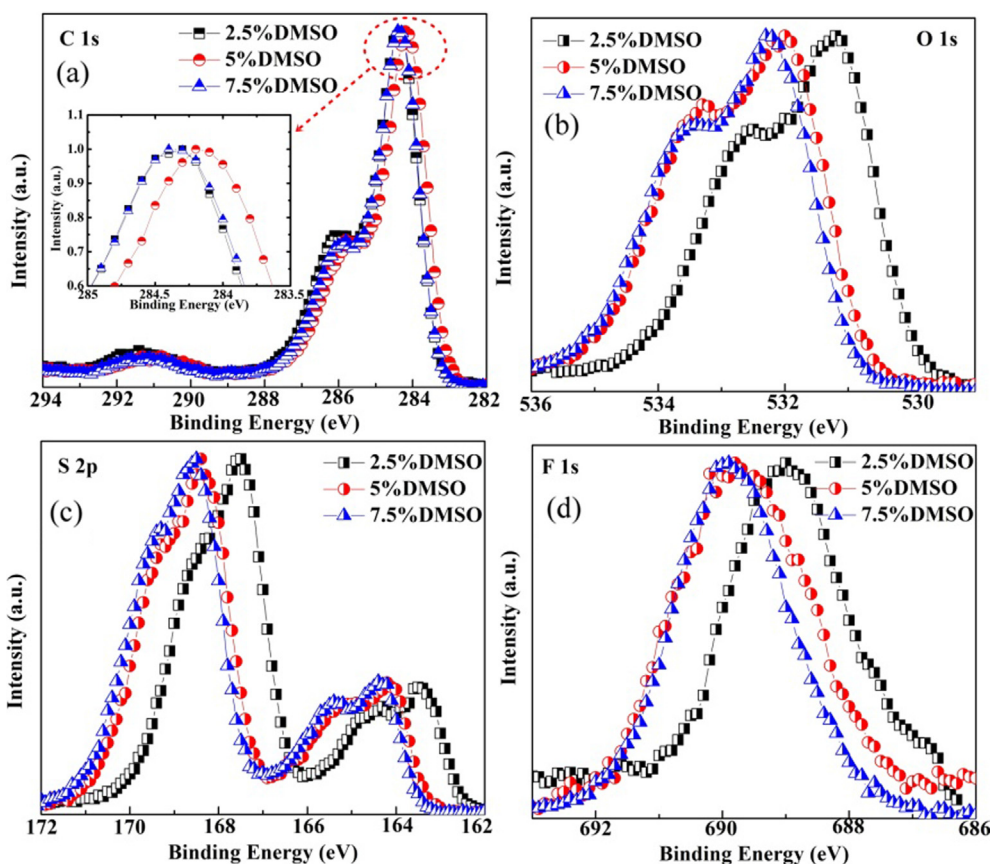


Fig. 5. The comparative bonding state [C 1s (a), O 1s (b) S 2p (c) and F 1s (d)] of different DMSO doped PEDOT:PSS films.

(0.37 eV). This indicates that the reduction of work function results a larger interface dipole [38] in the PEDOT:PSS/*n*-Si interface. We have observed larger open circuit voltage (V_{OC}) in 5% DMSO doped PEDOT:PSS/*n*-Si heterojunction solar cell which may occur due to the accumulation the larger number of charge carriers as a result of stronger interface dipole in this sample. Subsequently, this 5% DMSO doped PEDOT:PSS/*n*-Si heterojunction minimizes the charge recombination and can contribute to enhancing the hole injection into PEDOT:PSS layer. The electron affinity ($\chi_{PEDOT:PSS}$) of PEDOT:PSS with 5% DMSO doped thin film has been estimated from the band diagram and the value [shown in Fig. 6(c)] is similar to Prakoso et al. [39] report.

2.4. Electrical measurement

The electrical conductivity of different DMSO doped PEDOT:PSS thin films have been calculated by transmission length method (TLM) measurement. The schematic diagram of TLM is depicted in Fig. 7(a) and details calculation of TLM measurement is explained in the Supporting Information. The Current-Voltage measurement (different electrode spacing) of PEDOT:PSS thin film on glass is shown in insert Fig. 7(b), (c) and (d)]. Since R_T is linearly dependent on the intervals of distance, R_S and R_C can be extracted from the slope and intercept of the linear fit. Using R_T value for each distance interval d , we calculate the sheet resistance of the PEDOT:PSS films. Sheet resistance of 2.5% DMSO doped PEDOT:PSS thin film is maximum (338.7 Ω /sq) whereas minimum electrical conductivity is 540 S/cm. In 5% DMSO doped PEDOT:PSS film, we achieved the highest conductivity of 1230 S/cm due to the bigger domain length of PEDOT:PSS and thinner PSS surrounded on PEDOT as shown in Fig. 3. Further increase of DMSO (7.5%) the conductivity decreases again because of decrease of domain length and similar trend was obtained by Zhang et. al. [40] and Yeo et al. [41] We also compared the electrical conductivity of 5% DMSO

doped PEDOT:PSS thin film on glass and *n*-Si substrate by the same TLM method (shown in Fig. S3 in the Supporting Information). The conductivity of PEDOT:PSS is almost same on glass and *n*-Si substrate. Which suggest that most of the charge carriers are transported through the PEDOT:PSS domain.

2.5. Hybrid solar cell

The PEDOT:PSS thin film treated with different DMSO concentration is used as a hole transport layer in a hybrid organic/inorganic crystalline silicon solar cells. The active cell area is $1 \times 1 \text{ cm}^2$. The current density versus voltage ($J-V$) measurement of the fabricated PEDOT:PSS/*n*-Si hybrid solar cell was characterized under 1000 W/m^2 AM1.5 g standard illumination at 25 $^\circ\text{C}$, shown in Fig. 8. Highest open-circuit voltage (V_{OC}) of 560 mV is achieved for 5% DMSO doped PEDOT:PSS layer due to thinner PSS layer surrounded on PEDOT:PSS domain as discussed in XR and XPS/UPS analysis. However the V_{OC} is significantly less compare for the other DMSO doped PEDOT:PSS layer. The photovoltaic parameters of organic/inorganic hybrid solar cell are summarized in Table 1. As the conductivity of 5% DMSO doped PEDOT:PSS thin film is maximum (calculated from TLM measurement), so the effective series resistance is less (5.54 $\Omega \text{ cm}^2$) and short-circuit current density (J_{SC}) is high (29.7 mA/cm^2). As a result, the fill factor (FF) is enhanced (49.7%) and finally the overall PCE of 5% DMSO doped PEDOT:PSS/*n*-Si hybrid solar cell is maximum (8.5%) for unpassivated silicon substrate. [42] To improve the surface passivation of the crystalline silicon wafer and increase the effective lifetime of the minority carrier, an ultrathin ($\sim 5 \text{ nm}$) intrinsic amorphous silicon (a-Si:H) interlayer is deposited by PECVD before the PEDOT:PSS coating. Therefore current density-voltage response of these modified solar cell devices, showed an increase in open-circuit voltage from 560 to 600 mV due to reduce surface recombination velocity at the junction. Also the

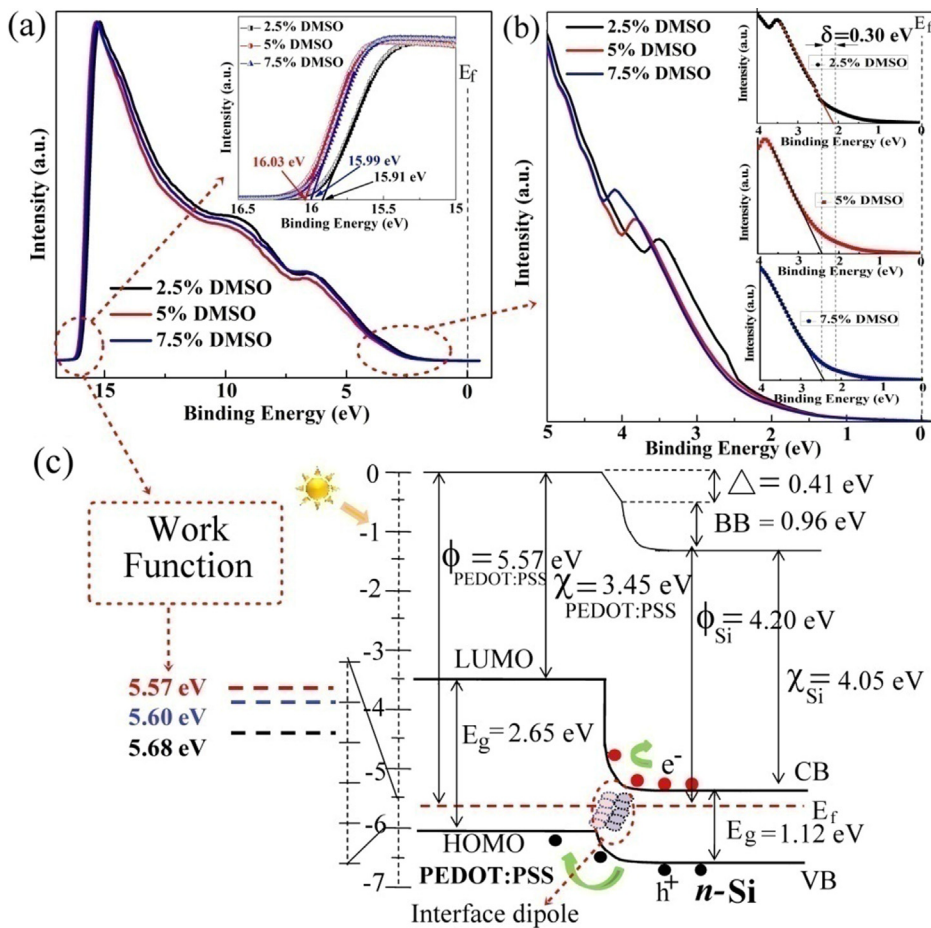


Fig. 6. (a) Ultraviolet photoelectron spectroscopy spectra of PEDOT:PSS/*n*-Si heterojunction (inset) indicates the value in binding energy of the secondary electron cut-off (SECO) (b) Magnified HOMO region of the PEDOT:PSS/*n*-Si heterojunction (inset) shows the shifted HOMO level of DMSO doped PEDOT:PSS and (c) Energy band extracted from UPS spectra of PEDOT:PSS/*n*-Si heterojunction solar cell where BB is band bending, Δ is the interface dipole, $\Phi_{\text{PEDOT:PSS}}$ & Φ_{Si} are the work function of PEDOT:PSS & *n*-type Si and χ is the electron affinity.

fill factor improved from 49.7% to 59.4%. Finally, the overall power conversion efficiency of 11.04% is achieved for the device with the passivating interlayer, as compared to 8.5% without it.

Also, the rectifying response indicates the junction behaves as a well-defined diode. So the dark current-voltage curve could be simulated according to the following equation:

$$J = J_s \left[\exp\left(\frac{q(V + JR_s)}{nKT}\right) - 1 \right] + \frac{V + JR_s}{R_p} \quad (2)$$

where n is the ideality factor, R_s the series resistance, R_p the parallel resistance, J_s the saturation current density, T is the temperature and K is the Boltzmann constant. The better performance of the front passivated silicon is also evident from the lower saturation current density (J_s) and the ideality factor closer to 1 ($n = 1.1$) of the 5% DMSO doped PEDOT:PSS/*n*-Si junction. Whereas, the higher ideality in un-passivated silicon ($n = 1.3$) indicates a stronger interface recombination owing to more interface defects at the PEDOT:PSS/*n*-Si junction extracted from fitting of the dark J - V response to the Schottky diode model (see the inset of Fig. 9). Therefore, the fill factor (FF) of 59.4% is higher for the passivated silicon, while un-passivated silicon has a considerably lower value of 49.7% of 5% DMSO doped PEDOT:PSS/*n*-Si hybrid solar cell.

To further characterized solar cells performance, the external quantum efficiency (EQE) was measured with a commercial equipment (PV Measurements). Fig. 9 shown the respective EQE response of different DMSO doped PEDOT:PSS layers, with a clear decrease in the mid-wavelength range, due to an increase of the reflection losses and to recombination losses at the rear surface. It has been seen that the light absorbed by 7.5% DMSO doped PEDOT:PSS film based hybrid solar cell is less than that of 2.5% DMSO doped PEDOT:PSS film based solar cell.

This indicates that the light reflected by 7.5% DMSO doped PEDOT:PSS film is more compared to the 2.5% DMSO doped PEDOT:PSS film (which is consistent with the top surface roughness obtained from the AFM measurements). Large light reflections probably produce a smaller number of electron-hole pairs and low short-circuit current density (J_{sc}) in the system. In the passivated silicon wafer the EQE spectra increased at > 300 nm to < 500 nm wavelength range compare to un-passivated silicon wafer. Therefore, the overall cell performance of passivated silicon is better including J_{sc} , FF, and efficiency.

The present study, in the step of 2.5% DMSO, clearly suggests that the 5% DMSO is the optimized condition. However, the actual value of DMSO may be 5% or slightly away (in either side) of 5%, which can only be estimated by preparing the films with DMSO in finer steps on both sides of the 5%. Without such fine checking, it can be inferred that the near 5% DMSO is the optimized condition.

3. Conclusions

The effect of DMSO on the structures (i.e. on the film thickness, EDPs and morphology) of PEDOT:PSS thin films and subsequently on the charge transport and performance of hybrid solar cell are shown. It is observed that 5% DMSO concentration exhibited the minimum film thickness due to less insulating PSS surrounded on PEDOT. As a result, the work function of PEDOT:PSS thin film is decreased by 0.12 eV and HOMO level is shifted by 0.3 eV to the higher binding energy. AFM analysis indicated that this 5% DMSO doped PEDOT:PSS thin film has maximum domain length of PEDOT:PSS as well as face-on orientation leading to superior charge transport pathways. Consequently, the electrical conductivity has been enhanced up to 1230 S/cm. The schematic block diagram, sketched by XR analysis and AFM topology, provides better understanding on the charge carrier transportation

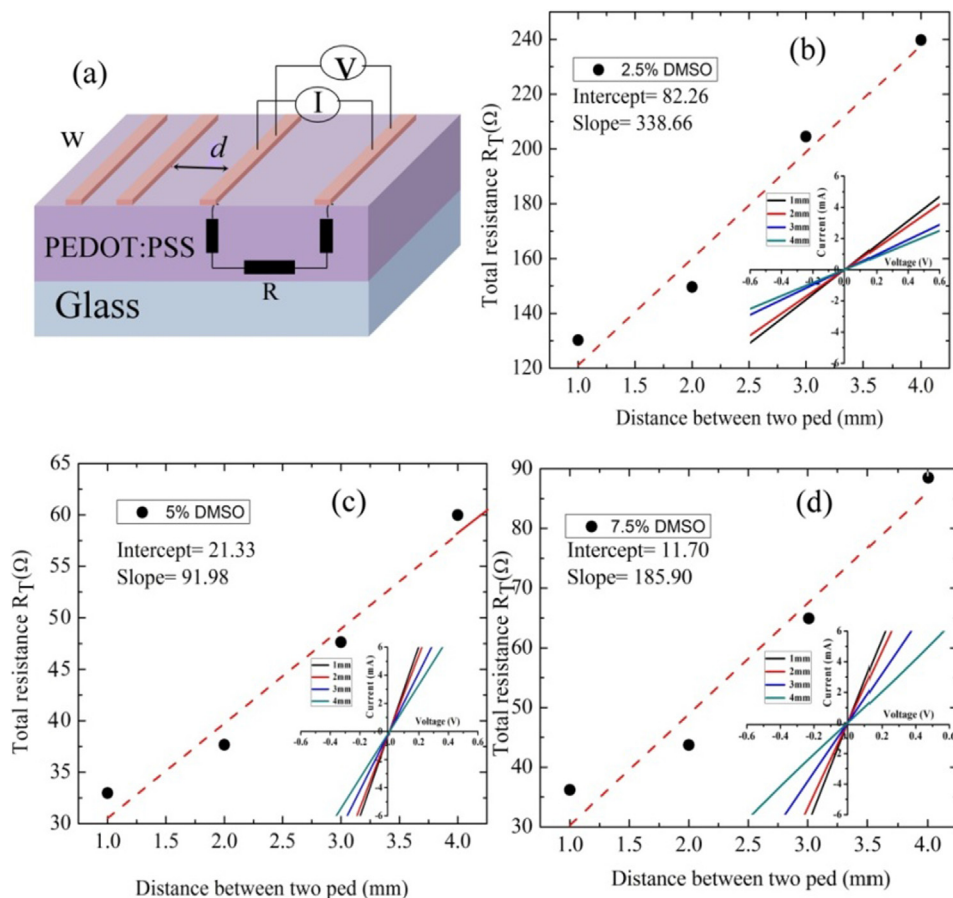


Fig. 7. (a) Schematic device structure of TLM, [(b), (c), (d)] TLM of different DMSO concentration doped PEDOT:PSS thin films over glass substrate.

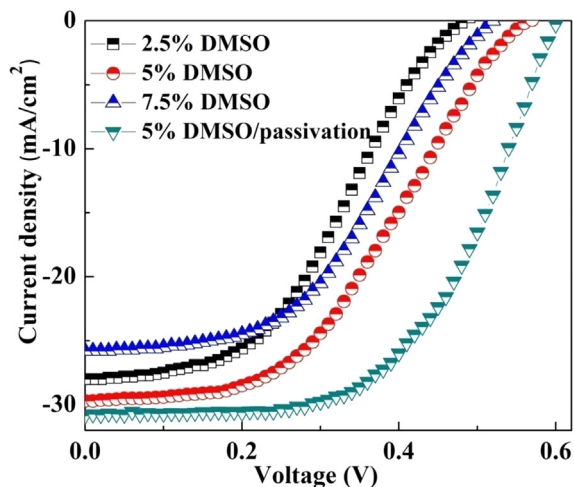


Fig. 8. Current density versus voltage characteristic of DMSO doped PEDOT:PSS/n-Si hybrid solar cells measured under 100 mW/cm² illumination (AM1.5).

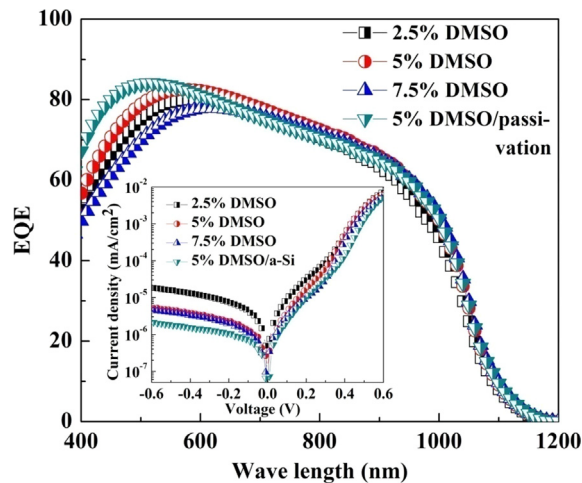


Fig. 9. EQE spectrum dependence on wavelength and (Insert) dark current density versus voltage characteristic of DMSO doped PEDOT:PSS/n-Si hybrid solar cells.

Table 1
Photovoltaic parameters of PEDOT:PSS/n-Si hybrid solar cell.

PEDOT:PSS	V_{OC} (mV)	FF (%)	J_{sc} (mA/cm ²)	PCE (%)	R_s (Ω -cm ²)
2.5% DMSO	487	36.8	28.01	5.01	8.90
5% DMSO	560	49.7	29.70	8.50	5.54
7.5% DMSO	521	42.4	25.88	5.70	8.48
5% DMSO/passivation	600	59.4	30.97	11.04	3.12

through PEDOT:PSS layer and effect of DMSO on the domains, which are very essential for the development of high efficiency hybrid solar cells and other optoelectronic application.

4. Experimental Section

4.1. Deposition of PEDOT:PSS thin film

PEDOT:PSS (PH1000) solution with 99.99% purity was purchased

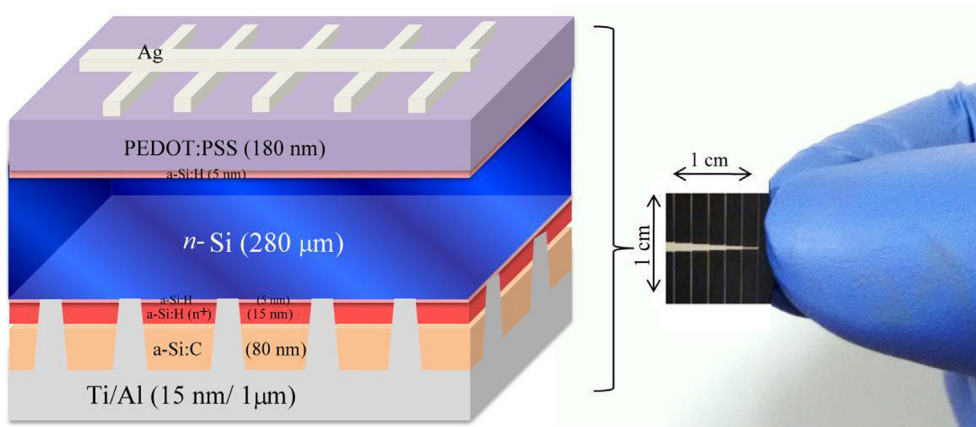


Fig. 10. Schematic block diagram of PEDOT:PSS/n-Si solar cell (beside) real device of $1 \times 1 \text{ cm}^2$ PEDOT:PSS/n-Si hybrid solar cell.

from Sigma Aldrich. Three different concentrations (2.5, 5 and 7.5 vol %) of DMSO (Sigma Aldrich) were mixed with the PEDOT:PSS solution. Afterwards, 0.1-vol% Capstone FS-31 was added to improve the final wettability of the PEDOT:PSS solution. Then spin coated with 1000 rpm for 60 s. The silicon substrates were cleaned by standard RCA cleaning techniques and then dip into 1% HF for 1 min and the glass substrates were cleaned by Ultrasonic Cleaning Bath (immersed in an acetone solution for 15 min then in an isopropyl alcohol for 15 min). After the deposition of DMSO doped PEDOT:PSS films were dried in air for a few minutes and then annealed on a hot plate for 30 min at 130°C in N_2 atmosphere.

4.2. Characterization of PEDOT:PSS thin film

4.2.1. X-ray reflectivity

The structures of the thin films were characterized using XR technique, which essentially provides an electron-density profile (EDP), i.e., in-plane ($x - y$) average electron density (ρ) as a function of depth (z) in high resolution [43–45] from which one can estimate the film-thickness, film-compactness, top and interface roughness. XR measurements of the films were carried out using a synchrotron source (MCX beamline, Elettra) [46] at wavelength, $\lambda = 1.24 \text{ \AA}$. The beamline is equipped with a diffractometer, which has a four-circle goniometer and a flat sample stage. The latter has two circular and three translational (X, Y, and Z) motions. Scattered intensities were recorded using a scintillator detector behind a set of receiving slits. Experimental data were taken in the specular condition; i.e., the reflected angle is equal to the incident angle (θ). Under such condition there exists a non-vanishing wave vector component, $q_z = (4\pi/\lambda) \sin \theta$, with resolution 0.001 \AA^{-1} .

4.2.2. Atomic force microscopy

The top surface morphology of the films was mapped using the AFM (5500 AFM, Agilent) technique. Topographic images were collected in a non-contact (or intermittence contact) mode to minimize the silicon-tip-induced damage of the soft film. Scans of different sizes and in different portions of the sample were carried out to get statistically meaningful information about the topography.

4.2.3. X-ray photoelectron spectroscopy

The electronic structure and interface property of PEDOT:PSS/n-Si was studied by XPS and UPS. The experiments were carried out using an Omicron Multi-probe (Omicron Nano Technology, UK) Ultrahigh vacuum (UHV) system (base pressure $\sim 2.0 \times 10^{-9}$ mbar), which is arrayed with an EA125 hemispherical electron analyzer and two light sources.

4.2.4. TLM measurement

Electrical conductivity was measured by transmission length method (TLM) using a Keithley 2400 source meter. Gold electrodes (50 nm thick) were deposited by thermal evaporation in a high vacuum process. Magnetic shadows masks were used to delimitate parallel contact electrodes ($1 \text{ cm} \times 1 \text{ mm}$). Spacing between electrodes ranged from 1 mm to 4 mm.

4.3. Solar cell fabrication

N-type float zone c-Si (100) double-side polished wafers, with a resistivity of $2.5 \Omega\text{-cm}$ and $280 \mu\text{m}$ in thickness, were used as the absorbing solar cell layer. The silicon substrates were cleaned using the standard RCA cleaning process and dipped in 1% HF acid during 1 min to remove native oxide. The backside of the solar cell, acting as electron selective contact, was fabricated by using a double layer stack. This stack consists of 5 nm hydrogenated amorphous silicon (a-Si:H) acting as a passivation layer followed by the deposition of 15 nm, n -doped a-Si:H layer acting as electron selective contact. Finally, an antireflection layer consisting of 80 nm hydrogenated amorphous silicon carbide (a-SiC:H) was deposited. Hydrogenated amorphous silicon layers were deposited by Plasma-Enhanced Chemical Vapor Deposition (PECVD) (13.56 MHz, 300°C). After that a nanosecond infrared laser fired contact (LFC) [47,48] was used to locally diffuse the n -dopant from the a-Si:H(n) layer into the crystalline silicon substrate, in order to ensure a good ohmic contact with the electron-beam evaporated Ti/Al (15 nm)/Al (1 μm) electrode. The front side of the solar cell, acting as hole selective contact, was fabricated using PEDOT:PSS compound. In particular, PEDOT:PSS solution (Clevios PH1000) mixed with three different DMSO concentration (2.5, 5 and 7.5 vol%) and 0.1% Capstone FS-31 (Dupont) was spin coated as discuss above. Finally, front electrode consisting of 150 nm thick Ag grid (4.3% shadow) was thermally evaporated using a magnetic shadow mask. Structure of the hybrid solar cell is shown in Fig. 10. Current density–voltage response of the solar cell was measured by means of a dc source meter (Keithley 2601B, USA) both in the dark and under AM1.5 g standard illumination (Oriel Instruments, USA) at 25°C (cell area was delimited by the use of an opaque mask).

Declaration of competing interest

The authors declare no competing financial interest.

Acknowledgements

The authors thank Dr. J. R. Plaisier and Dr. L. Gigli for their support in XR measurements. Authors are grateful to Dr. Ramkrishna Dev Das

and Mr. Goutam Sarkar for AFM, XPS/UPS. This work is partially supported by the Spanish government under the ENE2016-78933-C4-1-R and ENE2017-87671-C3-2-R projects. The financial support received by under Erasmus Mundus Action 2 AREAS+ grant programs is thankfully acknowledged. The financial support received by MM and SH under Indo-Italian POC to carry out XR experiments at Elettra is thankfully acknowledged.

Supplementary data

The Supporting Information contains thickness variation XR fitted plot, topology and phase AFM images, and calculation of TLM measurement. The following are the supplementary data related to this article. Supplementary data to this article can be found online at <https://doi.org/10.1016/j.apsusc.2019.143967>.

References

- [1] K. Kasahara, J. Hossain, D. Harada, K. Ichikawa, R. Ishikawa, H. Shirai, Crystalline-Si heterojunction with organic thin-layer (HOT) solar cell module using poly(3,4-ethylenedioxythiophene):poly(styrene sulfonate)(PEDOT:PSS), *Sol. Energy Mater. Sol. Cells* 181 (2018) 60.
- [2] S.S. Yoon, D.Y. Khang, High efficiency (> 17%) Si-organic hybrid solar cells by simultaneous structural, electrical, and interfacial engineering via low-temperature processes, *Adv. Ener. Mater.* 8 (2017) 1702655.
- [3] K. Sato, M. Dutta, N. Fukat, Inorganic/organic hybrid solar cells: optimal carrier transport in vertically aligned silicon nanowires arrays, *Nanoscale* 6 (2014) 6092.
- [4] J. Weickert, H. Sun, C. Palumbiny, H.C. Hesse, L.S. Mende, Spray-deposited PEDOT:PSS for inverted organic solar cells, *Sol. Energy Mater. Sol. Cells* 94 (2010) 2371.
- [5] D. Alemu, H.Y. Wei, K.C. Ho, C.W. Chu, Highly conductive PEDOT:PSS electrode by simple film treatment with methanol for ITO-free polymer solar cells, *Energy Environ. Sci.* 5 (2012) 9662.
- [6] Y. Kim, J. Lee, H. Kang, G. Kim, N. Kim, K. Lee, Controlled electro-spray deposition of highly conductive PEDOT:PSS films, *Sol. Energy Mater. Sol. Cells* 98 (2012) 39.
- [7] L. Huang, Z. Hu, K. Zhang, P. Chen, Y. Zhu, Dip-coating of poly(3,4-ethylenedioxythiophene):poly(styrenesulfonate) anodes for efficient polymer solar cells, *Thin Solid Film* 578 (2015) 161.
- [8] F. Zabihi, Y. Xie, S. Gao, M. Eslamian, Morphology, conductivity, and wetting characteristics of PEDOT:PSS thin films deposited by spin and spray coating, *Appl. Surf. Sci.* 338 (2015) 163.
- [9] J.G. Tait, B.J. Worfolk, S.A. Maloney, T.C. Hauger, A.L. Elias, J.M. Buriak, K.D. Harris, Spray coated high-conductivity PEDOT:PSS transparent electrodes for stretchable and mechanically-robust organic solar cells, *Sol. Energy Mater. Sol. Cell.* 110 (2013) 98.
- [10] Z. Yu, Y. Xia, D. Du, J. Ouyang, PEDOT:PSS films with metallic conductivity through a treatment with common organic solutions of organic salts and their application as a transparent electrode of polymer solar cells, *ACS Appl. Mater. Interfaces* 8 (2016) 11629.
- [11] Y.H. Kim, C. Sachse, M.L. Machala, C. May, L.M. Meskamp, K. Leo, Highly conductive PEDOT:PSS electrode with optimized solvent and thermal post-treatment for ITO-free organic solar cells, *Adv. Funct. Mater.* (21) (2011) 1076.
- [12] T. Stöcker, A. Köhler, R. Moos, Why does the electrical conductivity in PEDOT:PSS decrease with PSS content? A study combining thermoelectric measurements with impedance spectroscopy, *J. Polym. Sci. B Polym. Phys.* 50 (2012) 976.
- [13] T.R. Chou, S.H. Chen, Y.T. Chiang, Y.T. Lin, C.Y. Chao, Highly conductive PEDOT:PSS films by posttreatment with dimethyl sulfoxide for ITO-free liquid crystal display, *J. Mater. Chem. C* 3 (2015) 3760.
- [14] Y.J. Lin, W.S. Ni, J.Y. Lee, Effect of incorporation of ethylene glycol into PEDOT:PSS on electron phonon coupling and conductivity, *J. Appl. Phys.* 117 (2015) 215501.
- [15] Q. Liu, T. Imamura, T. Hiate, I. Khatri, Z. Tang, R. Ishikawa, K. Ueno, H. Shirai, Optical anisotropy in solvent-modified poly(3,4-ethylenedioxythiophene): poly(styrenesulfonic acid) and its effect on the photovoltaic performance of crystalline silicon/organic heterojunction solar cells, *Appl. Phys. Lett.* 102 (2013) 243902.
- [16] J. Ouyang, C.W. Chu, F.C. Chen, Q. Xu, Y. Yang, High-conductivity poly(3,4-ethylenedioxythiophene):poly(styrene sulfonate) film and its application in polymer optoelectronic devices, *Adv. Funct. Mater.* 15 (2005) 203.
- [17] X. Crispin, F.L.E. Jacobsson, A. Crispin, P. Grim, P. Andersson, A. Volodin, C.V. Haesendonck, M. Van der Auweraer, W.R. Salaneck, M. Berggren, The origin of the high conductivity of poly(3,4-ethylenedioxythiophene):poly(styrenesulfonate) (PEDOT:PSS) plastic electrodes, *Chem. Mater.* 18 (2006) 4354.
- [18] X. Wu, J. Liu, D. Wu, Y. Zhao, X. Shi, J. Wang, S. Huang, G. He, Highly conductive and uniform graphene oxide modified PEDOT:PSS electrodes for ITO-free organic light emitting diodes, *J. Mater. Chem. C* 2 (2014) 4044.
- [19] S. Dhar, T. Majumder, P. Chakraborty, S.P. Mondal, DMSO modified PEDOT:PSS polymer/ZnO nanorods Schottky junction ultraviolet photodetector: photoresponse, external quantum efficiency, detectivity, and responsivity augmentation using N doped graphene quantum dots, *Org. Electron.* 53 (2018) 101.
- [20] J.P. Thomas, L. Zhao, D. McGillivray, K.T. Leung, High-efficiency hybrid solar cells by nanostructural modification in PEDOT:PSS with co solvent addition, *J. Mater. Chem. A* 2 (2014) 2383.
- [21] I. Lee, G.W. Kim, M. Yang, T.S. Kim, Simultaneously enhancing the cohesion and electrical conductivity of PEDOT:PSS conductive polymer films using DMSO additives, *ACS Appl. Mater. Interfaces* 8 (2016) 302.
- [22] M. Pietsch, S. Jackle, S. Christiansen, Interface investigation of planar hybrid n-Si/PEDOT:PSS solar cells with open circuit voltages up to 645 mV and efficiencies of 12.6%, *Appl. Phys. A Mater. Sci. Process.* 115 (2014) 1109.
- [23] R. Liu, S.T. Lee, B. Sun, 13.8% efficiency hybrid Si/organic heterojunction solar cells with MoO₃ film as antireflection and inversion induced layer, *Adv. Mater.* 26 (2014) 6007.
- [24] Q. Liu, M. Ono, Z. Tang, R. Ishikawa, K. Ueno, H. Shirai, Highly efficient crystalline silicon/Zonylfluorosurfactant-treated organic heterojunction solar cells, *Appl. Phys. Lett.* 100 (2012) 183901.
- [25] K.A. Nagamatsu, S. Avasthi, J. Jhaveri, J.C. Sturm, 12% efficient silicon/PEDOT:PSS heterojunction solar cell fabricated at < 100 °C, *IEEE J. Photovoltaics* 4 (2014) 260.
- [26] J.P. Thomas, K.T. Leung, Mixed co-solvent engineering of PEDOT:PSS to enhance its conductivity and hybrid solar cell properties, *J. Mater. Chem. A* 4 (2016) 17537.
- [27] L.G. Parratt, Surface studies of solids by Total reflection of X-rays, *Phys. Rev.* 95 (1954) 359.
- [28] J.K. Bal, S. Hazra, Interfacial role in room-temperature diffusion of Au into Si substrates, *Phys. Rev. B* 75 (2007) 205411.
- [29] D.A. Mengistie, P.C. Wang, C.W. Chu, Effect of molecular weight of additives on the conductivity of PEDOT:PSS and efficiency for ITO-free organic solar cells, *J. Mater. Chem. A* 1 (2013) 9907.
- [30] J. Rivnay, S. Inal, B.A. Collins, M. Sessolo, E. Stavrinidou, X. Strakosas, C. Tassone, D.M. Delongchamp, G.G. Malliaras, Structural control of mixed ionic and electronic transport in conducting polymers, *Nat. Commun.* 7 (2016) 11287.
- [31] D.A. Mengistie, C.H. Chen, K.M. Boopathi, F.W. Pranoto, L.J. Li, C.W. Chu, Enhanced thermoelectric performance of PEDOT:PSS flexible bulky papers by treatment with secondary dopants, *ACS Appl. Mater. Interfaces* 7 (2015) 94.
- [32] S. Mahato, Composition analysis of two different PEDOT:PSS commercial products used as an interface layer in Au/n-Si Schottky diode, *RSC Adv.* 7 (2017) 47125.
- [33] H.K. Park, S.H. Lee, F.S. Kim, H.H. Choi, I.W. Cheong, J.H. Kim, Enhanced thermoelectric properties of PEDOT:PSS nanofilms by a chemical dedoping process, *J. Mater. Chem. A* 2 (2014) 6532.
- [34] D.J. Yun, H. Ra, J. Kim, I. Hwang, J. Lee, S.W. Rhee, J.G. Chunga, Characterizing annealing effect of poly(3,4-ethylenedioxythiophene) polymerized with poly(4-styrenesulfonate) conjugated film on the molecular arrangement and work function by Core-level and valence-level band spectra, *ECS J. Solid State Sci. Technol.* 1 (2012) 10.
- [35] A. Nardes, M.M. Kemerink, M.M. Kok, E. Vinken, K. Maturova, R.A.J. Janssen, Conductivity, work function, and environmental stability of PEDOT:PSS thin films treated with sorbitol, *Org. Electron.* 9 (2008) 727.
- [36] A. Kanwat, J. Jang, High work function with reduced phase separation of PSS in metal oxide modified PEDOT:PSS interlayers for organic photovoltaics, *RSC Adv.* 6 (2016) 114800.
- [37] S.I. Na, G. Wang, S.S. Kim, T.W. Kim, S.H. Oh, B.K. Yu, T. Lee, D.Y. Kim, Evolution of nanomorphology and anisotropic conductivity in solvent-modified PEDOT:PSS films for polymeric anodes of polymer solar cells, *J. Mater. Chem.* 19 (2009) 9045.
- [38] S. Park, Y. Yi, S.W. Cho, H. Lee, Work function reduction using 8 hydroxyquinolinolato-lithium for efficient inverted devices, *Chem. Phys. Lett.* 652 (2016) 102.
- [39] A.B. Prakoso, Rusli, Z. Li, C. Lu, C. Jiang, Design guideline for Si/organic hybrid solar cell with interdigitated back contact structure, *Semicond. Sci. Technol.* 33 (2018) 035016.
- [40] S. Zhang, P. Kumar, A.S. Nouas, L. Fontaine, H. Tang, F. Ciccoira, Solvent-induced changes in PEDOT:PSS films for organic electrochemical transistors, *APL Mater* 3 (2015) 014911.
- [41] J.S. Yeo, J.M. Yun, D.Y. Kim, S. Park, S.S. Kim, M.H. Yoon, T.W. Kim, S.I. Na, Significant vertical phase separation in solvent-vapor-annealed poly(3,4-ethylenedioxythiophene):poly(styrene sulfonate) composite films leading to better conductivity and work function for high-performance indium tin oxide-free optoelectronics, *ACS Appl. Mater. Interfaces* 4 (2012) 2551.
- [42] S. Mahato, L.G. Gerling, C. Voz, R. Alcubilla, J. Puigdollers, High efficiency ITO-free hybrid solar cell using highly conductive PEDOT:PSS with co-solvent and surfactant treatments, *Mater. Lett.* 186 (2017) 165.
- [43] M. Mukhopadhyay, S. Hazra, Growth of thiol-coated Au-nanoparticle Langmuir monolayers through a 2D-network of disk-like islands, *RSC Adv.* 6 (2016) 12326.
- [44] I. Roy, S. Hazra, Structures of spin-coated and annealed monolayer and multilayer poly(3-dodecylthiophene) thin films, *RSC Adv.* 7 (2017) 2563.
- [45] M. Mukhopadhyay, S. Hazra, Interfacial and thermal energy driven growth and evolution of Langmuir-Schaefer monolayers of Au-nanoparticles, *Phys. Chem. Chem. Phys.* 20 (2018) 1051.
- [46] I. Ahmed, L. Dildar, A. Haque, P. Patra, M. Mukhopadhyay, S. Hazra, M. Kulkarni, S. Thomas, J.R. Plaisier, S.B. Dutta, J.K. Bal, Chitosan-fatty acid interaction mediated growth of Langmuir monolayered Langmuir-Blodgett films, *J. Colloid Interf. Sci.* 514 (2018) 433.
- [47] P. Ortega, A. Orpella, I. Martín, M. Colina, G. López, C. Voz, M.I. Sánchez, C. Molpeceres, R. Alcubilla, Laser-fired contact optimization in c-Si solar cells, *Prog. Photovolt. Res. Appl.* 20 (2012) 173.
- [48] J. He, S. Hegedus, U. Das, Z. Shu, M. Bennett, L. Zhang, R. Birkmire, Laser-fired contact for n-type crystalline Si solar cells, *Prog. Photovolt. Res. Appl.* 23 (2015) 1091.